NOx production in plasma reactors by pulsed spark discharges

1   # NOx production in plasma reactors by pulsed spark discharges

2

3   **Jing Li, Shuiliang Yao* and Zuliang Wu***

4   School of Environmental and Safety Engineering, Changzhou University, Changzhou 213164,

5   People's Republic of China

6   E-mail: yaos@cczu.edu.cn (S Yao); wuzuliang@cczu.edu.cn (Z Wu)

7

8   **Abstract**

9   Nitrogen fertilizers are important for modern agriculture, among which nitric acid is a basic

10   chemical for ammonium nitrate production. Herein, NOx was produced from N_2 and O_2 using a

11   spark discharge technology with point-to-point and circle-to-plate types of plasma reactors

12   driven by a nano-second pulsed power supply. NOx could be produced with an energy

13   efficiency of 0.09 mol/kWh under the gases of 50%/50% N_2/O_2, while NO_2 selectivity

14   increased with increasing energy density. The gas temperatures in the spark channels were

15   estimated using the Gibbs free energy equation. Based on kinetics calculations, the reactions of

16   N with O_2 and O with NO were the major reactions for NOx production.

17

20

1

1. Introduction

Nitrogen is an important element in fertilizers, accounting for nearly 50% of fertilizers [1]. Nitrogen fertilizers are essential for food production. Although nitrogen is abundant in the atmosphere, it is difficult to utilize because of the high activation energy barrier caused by the extremely stable N≡N triple bonds [2]. Normally, nitrogen is fixed with hydrogen to produce ammonia at 773–873 K and under 17–20 MPa through the Haber–Bosch (HB) process. Nearly 97% of nitrogen fertilizers are derived from synthetically produced ammonia, including urea, $NH_4(OH)$, and NH_4NO_3 [3-5]. Nitrogen fertilizers significantly increase agricultural productivity, which sustains nearly half of the world's population [6]. Nevertheless, fertilizers are generally produced in a chemical plant and transported to the agricultural areas where the fertilizers are stored and used [7]. The transportation and storage of the fertilizers create new environmental risks. Modern agricultural, environmental, and ecological technologies require fertilizers to be produced onsite [8].

Recently, attention has been given to the exploitation of low-temperature plasma technologies to produce nitrogen oxides (NOx) for agricultural applications, which are related to active nitrogen and oxygen species [9,10]. Meanwhile, aqueous HNO_3 can be facilely produced using NO_2 and H_2O [6]. The acidic solution can further react with volatile NH_3, which is naturally created by bacteria, to generate ammonium nitrate. Thus, organic fertilizers with a high N content per mass (35%) can be achieved. Compared to the high temperatures and

2

1   pressures of the HB process, plasma nitrogen fixation offers an opportunity to produce NOx

2   onsite at room temperature and atmospheric pressure.

3   In the past decades, various plasma technologies, such as glow, spark, arc, and dielectric

4   barrier discharge, have been reported in the field of NOx production [2,6,11]. For spark

5   discharge, the discharge voltage can initially increase up to a high value of 20 kV, accompanied

6   by a high energy efficiency of 0.02 mol/kWh [6,12,13]. The ultrafast repetitive discharge

7   processes facilely induce ultrahigh electron energies, which are beneficial for activating and

8   dissociating gas molecules [14-16]. Based on our previous studies of methane oxidation

9   [17-21], high energy efficiency of methane conversion can be achieved from 2.5 to 14.4

10 mol/kWh by pulsed spark discharge at a relatively low energy density, and plasma reactors can

11 be readily distributed on farms. Therefore, plasma technology provides a potential route for the

12 onsite production of nitrogen fertilizers.

13   In this work, NOx production using a nano-second pulsed spark discharge was investigated.

14 The pulsed spark discharge occurred between two electrode terminals in point-to-point (PTP)

15 and the circle-to-plate (CTP) reactors. The two reactors were characterized by different energy

16 densities. The temperatures of the gases in the spark channels were estimated using the Gibbs

17 free energy (GFE) equation. The mechanism of NOx production was proposed based on

18 kinetics calculations.

19

20

3

1   **2. Experimental system and data analysis**

2   Figure 1 shows the experimental setup consisting of a pulse power supply (DP-15K35, Peec,

3   Japan), a plasma reactor, and an electrical measurement system. The pulse power supply could

4   provide voltage pulses with a repetition frequency from 50 Hz to 35 kHz. The discharge

5   voltage and current signals were measured using a voltage probe (EP-50K, Peec, Japan) and a

6   current transformer (mode 0.5–1.0, Strangenes Industries, USA) and were recorded with a

7   digital oscilloscope (TDS754D, Tektronix, USA) with an analog bandwidth of 1 GHz.

8   Two plasma reactors of different geometric structures were designed based on our previous

9   work [17,18]. A PTP type of reactor is consisted of a Pyrex® tube $(1.5\times10^{-2}$(o.d.)

10    $\times1.2\times10^{-2}$(i.d.) $\times0.8$(length) $m^3)$, a quartz tube $(1.2\times10^{-2}$(o.d.) $\times8.0\times10^{-3}$(i.d.) $\times0.4$(length) $m^3)$,

11   and two stainless-steel wire electrodes (HV and ground, $\Phi1.5\times10^{-3}$ $\times0.18$(length) $m^2)$ with

12   sharp-pointed discharge terminals. The gap distance between the two electrodes is 2×10^{-3} m

13   (Figure 1A). The position of the spark discharge channel is fixed between two electrode

14   terminals in the PTP reactor.

15   Figure 1B shows the configuration of a CTP type of reactor and the gas stream paths. The

16   CTP reactor is consisted of a quartz tube $(1.2\times10^{-2}$(o.d.) $\times1.0\times10^{-2}$(i.d.) $\times0.4$(length) $m^3)$, a

17   stainless-steel tube (HV, 6×10^{-3}(o.d.) $\times4\times10^{-3}$(i.d.) $m^2)$, and a stainless-steel cap (ground,

18    $\Phi8\times10^{-3}$ m). The discharge gap is fixed at 1×10^{-3} m. In contrast, a CTP type of reactor, the

19   spark discharge channel is confined in the limited space between the plate and the circle of the

20   tube end; the space is larger than that of the PTP reactor. Meanwhile, there are relatively

4

1   uniform discharges across the gas flow in the CTP reactor, not like the PTP reactor that has a

2   large part of space without discharges.

3
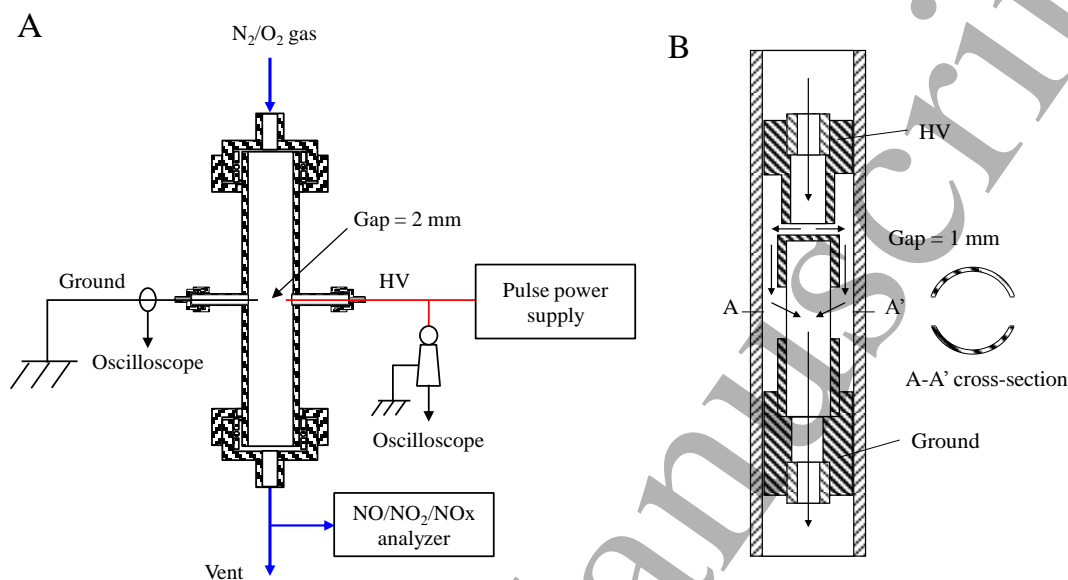
4

5   **Figure 1.** (A) Pulsed spark discharge system for NOx production in the PTP reactor and (B) the

6   detailed configuration of the CTP reactor.

7

8   A gas mixture of 50% N_2 and 50% O_2 was introduced into the upper part of the vertically

9   oriented reactor at a total flow rate $F_0 = 0.2$ L/min. The NO_2 and NO concentrations in mg/Nm^3

10   (where the gas state was 298 K and 1 atm) were measured using a nitrogen oxide analyzer

11   (ECL-880US, Yanaco, Japan), which was based on chemiluminescence.

12   The energy injection E in J/pulse from the pulse power supply to the reactor was calculated

13   as follows:

$$E = \sum_{i=0}^{n} \left(\frac{V_i + V_{i+1}}{2}\right)\left(\frac{I_i + I_{i+1}}{2}\right)(t_{i+1} - t_i), \tag{1}$$

5

1   where V_i, V_{i+1} in V and I_i, I_{i+1} in A were the discharge voltage and current at discharge time t_i

2   and t_{i+1} in s, respectively. The discharge voltage and current were obtained from the data

3   sequences of the discharge voltage and current waveforms. The discharge power in W was the

4   product of the energy injection and pulse repetition frequency f in Hz.

5   The energy density in J/L was defined as the ratio of the discharge power to the total gas flow

6   rate F_0 at 298 K in L/min, described as follows:

$$\text{Energy density} = \frac{60E}{F_0} \times f. \tag{2}$$

7   The energy efficiency in mol/kWh was defined as a ratio of moles of produced NOx per hour

8   to the amount of the discharge power into the mixture gases:

$$\text{Energy efficiency} = \frac{1000 \times [\text{moles of NOx production per hour}]}{E \times f}. \tag{3}$$

9   The selectivity of NO_2 was defined as follows:

$$S_{NO_2} = \frac{[NO_2]}{[NO_2] + [NO]} \times 100\%, \tag{4}$$

10   where $[NO_2]$ and $[NO]$ were the concentrations of NO_2 and NO in the outlet gases of the

11   plasma reactors, respectively.

12

13   **3. Results and discussions**

14   3.1. Typical waveforms of discharge voltage and current

15   The pulse power supply was utilized to generate the pulsed spark discharges between the

16   electrode pairs, resulting in the formation of a spark channel. The gases in the spark channel

17   were rapidly elevated to a high temperature and then decomposed. Figure 2 shows the

6

1   time-resolved voltage and current profiles over a single-pulse spark discharge in the PTP and

2   CTP reactors, respectively. They show that the pulse rise time and the full width at half

3   maximum (FWHM) values of the voltage and current in the PTP and CTP reactors were within

4   dozens of nanoseconds (Table 1). The pulse width has an impact on the process of NOx

5   production during the pulsed spark discharge. When the pulse width is small and the

6   instantaneous input power is large, the gas temperature in the spark channels will be high,

7   which is conducive to the generation of NOx. The peak values of the voltage and current of the

8   pulsed spark discharge in the PTP reactor were 6.8 kV and 57.7 A, respectively, while those in

9   the CTP reactor were 6.8 kV and 60.4 A, respectively. The energy injections in the PTP and

10   CTP reactors were 0.00369 and 0.00339 J/pulse, respectively.

11

1
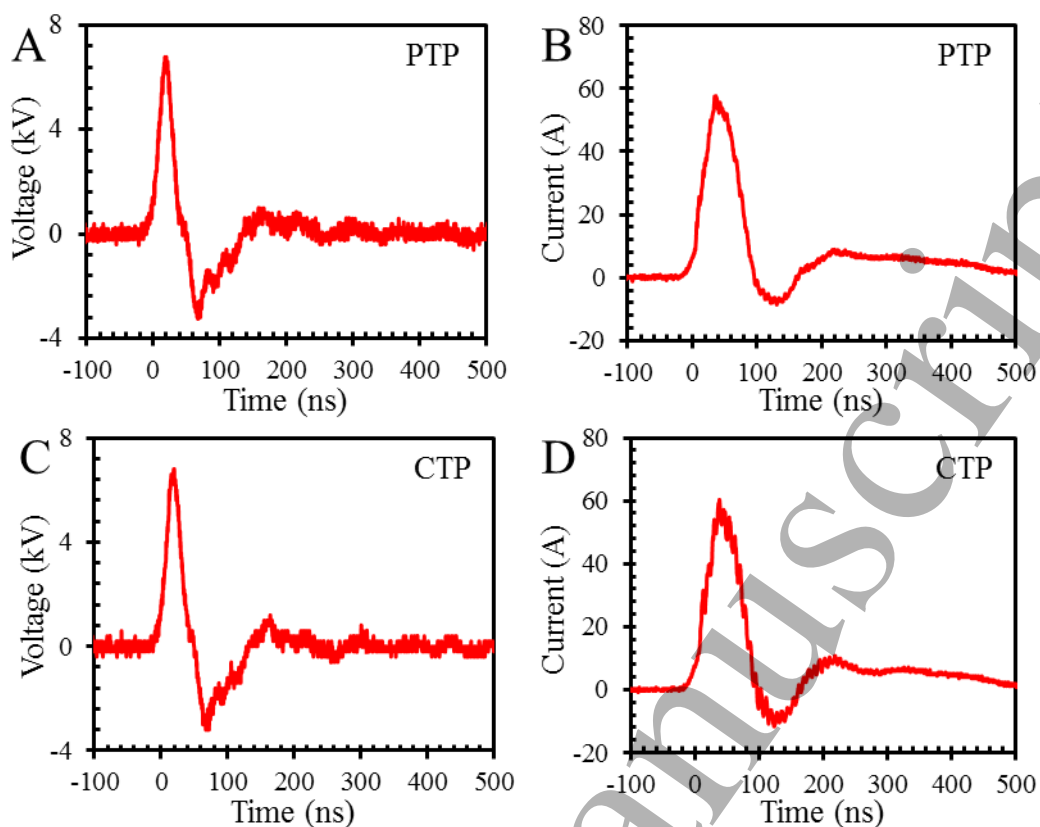
2   **Figure 2.** Voltage and current curves of the pulsed speak discharge in the (A, B) PTP and the

3   (C, D) CTP reactors.

4

5   **Table 1.** Electrical properties of the pulsed spark discharge in the plasma reactors.

Reactor	Voltage			Current			E
	Rise time	FWHM	Peak value	Rise time	FWHM	Peak value	
	(ns)	(ns)	(kV)	(ns)	(ns)	(A)	(J/pulse)
PTP	17.2	23.7	6.8	32.5	57.4	57.7	0.00369
CTP	22.0	22.4	6.8	38.4	55.6	60.4	0.00339

6

1   3.2. Energy efficiency of NOx production

2   The NOx production at various energy densities in the PTP and CTP reactors were illustrated

3   in Figure 3. The NOx concentration increased with increasing energy density. In the PTP

4   reactor, the NO_2 concentration increased from 175 to 2002 mg/Nm^3 as the energy density

5   increased from 331 to 6094 J/L, while that in the CTP reactor increased from 230 to 1417

6   mg/Nm^3 as the energy density increased from 275 to 2811 J/L. The energy efficiencies of the

7   pulsed spark discharges in the PTP and CTP reactors for NOx production were further

8   calculated and shown in Figure 4A. The energy efficiency in the PTP reactor achieved a high

9   level of 0.09 mol/kWh at an energy density of 331 J/L, while that in the CTP reactor was 0.09

10   mol/kWh at a low energy density of 275 J/L. However, the energy efficiency in the plasma

11   reactors decreased with increasing energy density. Normally, the NO_2 selectivity is a crucial

12   factor for the synthesis of aqueous HNO_3, the NO_2 selectivity in the PTP and CTP reactors

13   were shown in Figure 4B. The NO_2 selectivity increased with increasing energy density in the

14   plasma reactors, when the input gases were consisted of 50%/50% O_2/N_2. It had nearly 80%

15   NO_2 selectivity when the energy density was above 3000 J/L. The results in this study are

16   contrary to the reported one [22], which was conducted by atmospheric air. The different

17   ratios of input gases may be one reason for the different experimental results. The details

18   were analyzed based on kinetics calculations in the following.

19

20

9
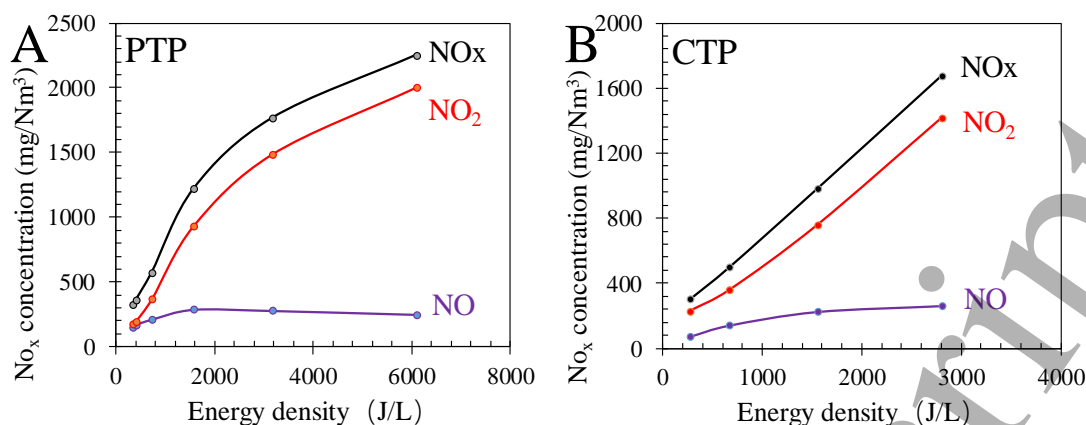
2   **Figure 3.** NOx concentration at various energy densities in the (A) PTP and (B) CTP reactors.
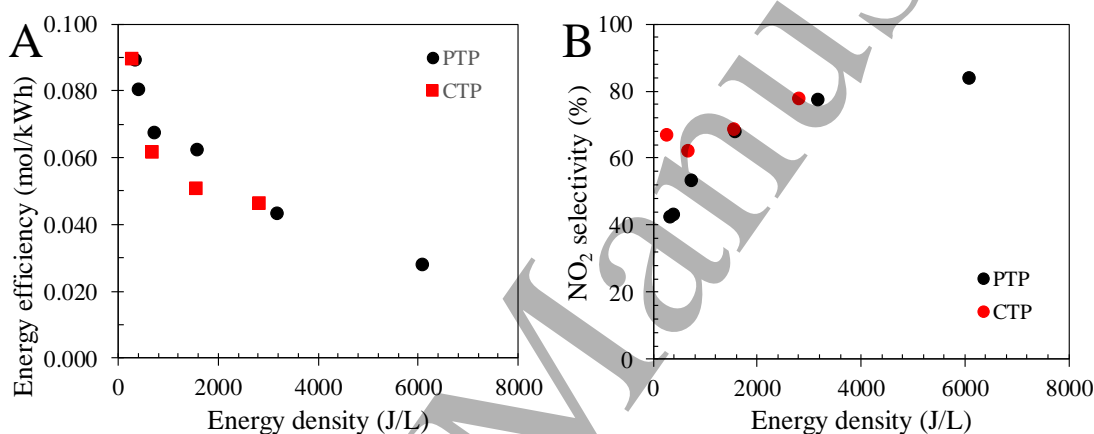
5   **Figure 4.** (A) Energy efficiency of NOx production and (B) NO_2 selectivity at various energy

6   densities in the PTP and CTP reactors.

8   3.3. Estimation of gases temperatures in the spark channel

9   The increase in the discharge power leads to the increase in the temperature of the gases in the

10   spark channel, which will simultaneously promote the increase of vibrational and rotational

11   temperatures and the decrease of the activation energies of reactions. Thus, it shifts the reaction

12   toward NOx production in the following reaction:

10

$$N_2 + O_2 = 2NO. \tag{5}$$

1   The equilibrium constant K (Eq. 6) for the NOx formation reaction depends on the reaction

2   temperature, and thus, the Gibbs free energy equation (Eq. 7) can be used to estimate the

3   reaction temperature T_K:

$$K = \frac{[NOx]^2}{[N_2][O_2]}, \tag{6}$$

$$\Delta G = -RT_K \ln K, \tag{7}$$

4   where ΔG was the Gibbs free energy, K was the equilibrium constant.

5   Here, $\Delta G = 86.55$ kJ/mol [23]. The equilibrium constant K can be calculated from the NOx

6   concentration data in Figure 3. The gas temperature T_K during the pulsed spark discharges in

7   the PTP and CTP reactors by using the GFE equation was displayed in Figure 5. The highest

8   temperatures of the background gases through the plasma space of the PTP and CTP reactors

9   were 2417 and 2147 K, respectively.

10

11

12

13

11

1
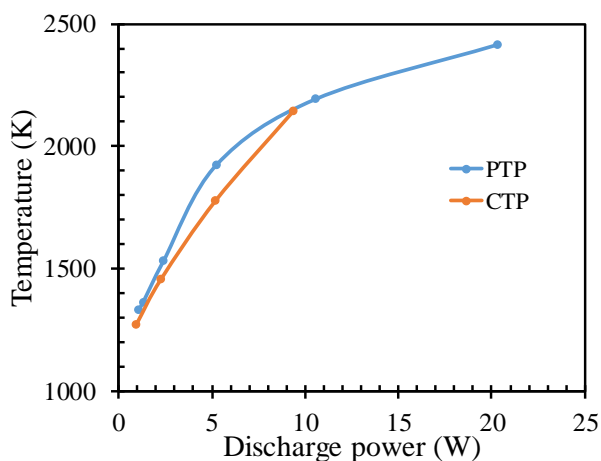
2 **Figure 5.** Temperature of gases through the plasma space of the PTP and CTP reactors plotted

3 as a function of the discharge power using the GFE equation. (Calculation conditions: E =

4 0.00369 J/pulse when the voltage and current peak values were 6.8 kV and 57.7 A, respectively,

5 in the PTP reactor; E = 0.00339 J/pulse when voltage and current peak values were 6.8 kV and

6 60.4 A, respectively, in the CTP reactor).

7

8 3.4. Kinetics of NOx production reactions

9 To further understand the NOx production processes from 50% N_2 and 50% O_2 during the

10 pulsed spark discharges, the kinetics calculations of the NOx production reactions were studied.

11 The two-temperature kinetics mechanism and rates [24] were used to predict the temporal

12 evolution and corresponding steady-state species. During the pulsed spark discharges, oxygen

13 and nitrogen atoms were initially formed from the decomposition of oxygen and nitrogen

14 molecules, respectively (Eqs. 8 and 9) [25,26]:

$$O_2+e \rightarrow 2O+e, \tag{8}$$

$$N_2+e \rightarrow 2N+e. \tag{9}$$

12

1   The decomposition rates $-r$ were calculated using Eqs. 10 and 11, where the rate

2   coefficient k was modeled through an Arrhenius-type equation (Eq. 12) [27]:

$$-r_{O_2} = k_{O_2}[O_2][e], \ k_{O_2} = 2.85 \times 10^{17} T_e^{-0.6} e^{\frac{-59500}{T_e}} \ (\text{cm}^3 \ \text{mol}^{-1} \ \text{s}^{-1}), \tag{10}$$

$$-r_{N_2} = k_{N_2}[N_2][e], \ k_{N_2} = 1.18 \times 10^{18} T_e^{-0.7} e^{\frac{-113200}{T_e}} \ (\text{cm}^3 \ \text{mol}^{-1} \ \text{s}^{-1}), \tag{11}$$

$$k = A \cdot T^n \cdot exp\left(\frac{-E_a}{T}\right), \tag{12}$$

3   where k in $\text{cm}^3 \ \text{mol}^{-1} \ \text{s}^{-1}$ was the rate coefficient, A was the values for the pre-exponential

4   factor, n was exponent, E_a was the activation energy.

5   Figure 6A shows the rate coefficients for Eqs. 8 and 9 at various electron temperatures. The

6   rate coefficient of O_2 decomposition was higher than that of N_2 decomposition. Figure 6B

7   displays the ratio α_1, defined as follows:

$$\alpha_1 = \frac{-r_{O_2}}{-r_{O_2} + -r_{N_2}} = \frac{k_{O_2}[O_2]}{k_{O_2}[O_2] + k_{N_2}[N_2]}, \tag{13}$$

8   where the ratio α_1 means the decomposition ratio of active oxygen and nitrogen molecules at

9   various electron temperatures.

10   It is known that the electron temperature is generally between 1 to 20 eV in an atmospheric

11   plasma [28], thus, the content of active oxygen atoms is higher than that of active nitrogen

12   atoms during the discharge processes when the same concentrations of O_2 and N_2 were input.

13

13
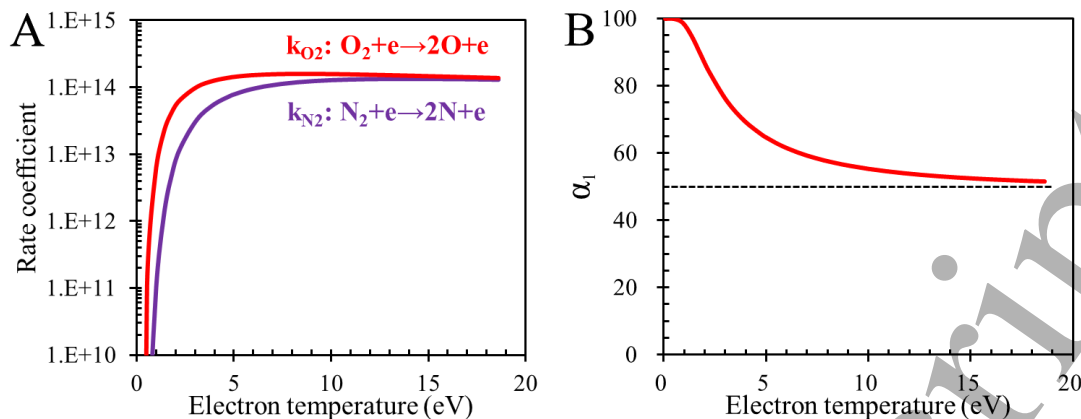
Figure 6. (A) Rate coefficients of Eqs. (8) and (9) plotted as functions of the electron temperature and (B) corresponding rate ratio at different electron temperatures.

According to the Zeldovich mechanism of the NO formation reactions [29,30], the rate coefficients of Eqs. 14 and 15

$$O+N_2 \rightarrow NO+N, \tag{14}$$

$$N+O_2 \rightarrow NO+O, \tag{15}$$

$$-r_O = k_O[O][N_2], k_O = 1.8 \times 10^8 e^{\frac{-38370}{T}} \text{ (cm}^3 \text{ mol}^{-1} \text{ s}^{-1}), \tag{16}$$

$$-r_N = k_N[N][O_2], k_N = 1.8 \times 10^4 e^{\frac{-4680}{T}} \text{ (cm}^3 \text{ mol}^{-1} \text{ s}^{-1}), \tag{17}$$

at different reaction temperatures were compared in Figure 7A.

When the temperature was below 3647 K, the reaction of N and O_2 was the main reaction. On the contrary, the reaction of O and N_2 became the prominent reaction when the temperature increased to 3647 K. The reaction rate ratio α_2 was defined as follows:

$$\alpha_2 = \frac{-r_N}{-r_O + -r_N} = \frac{k_N[N][O_2]}{k_O[O][N_2] + k_N[N][O_2]}, \tag{18}$$

14

1   which was calculated and shown in Figure 7B. The ratio α_2 means which is the main reaction

2   between the reactions Eqs. 14 and 15 according to the Zeldovich mechanism of the NO

3   formation at different temperatures. Typically, α_2 is 90% at 2882 K for the same

4   concentrations of input N_2 and O_2. As it was estimated using the GFE equation, the reaction

5   temperature was around 2400 K in the discharge channels, where the NO was mainly from the

6   reaction of N with O_2.

7
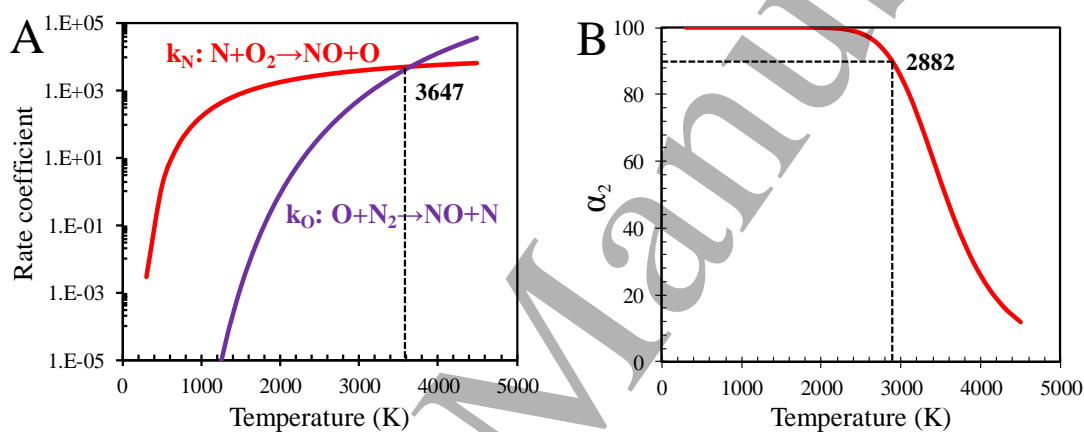
9   **Figure 7.** (A) Rate coefficient of Eqs. (14) and (15) at different temperatures and (B)

10 corresponding reaction rate ratio at different temperatures.

11

12 Furthermore, the possible reaction routes for active O according to previous works [27,31]

13 were evaluated as follows:

$$O_1: O+NO+M \rightarrow NO_2+M, \tag{19}$$

$$O_2: O+O+M \rightarrow O_2+M, \tag{20}$$

$$O_3: O+O_2+M \rightarrow O_3+M. \tag{21}$$

15

1   The rate coefficients of these three reactions at different reaction temperatures were

2   calculated as follows:

$$-r_{O_1} = k_{O_1}[O][NO][M], k_{O_1} = 1.83 \times 10^{20} T^{-1.63} \text{ (cm}^3 \text{ mol}^{-1} \text{ s}^{-1}), \tag{22}$$

$$-r_{O_2} = k_{O_2}[O][O][M], k_{O_2} = 1.89 \times 10^7 e^{\frac{-898}{T}} \text{ (cm}^3 \text{ mol}^{-1} \text{ s}^{-1}), \tag{23}$$

$$-r_{O_3} = k_{O_3}[O][O_2][M], k_{O_3} = 10^{13} e^{\frac{-204}{T}} \text{ (cm}^3 \text{ mol}^{-1} \text{ s}^{-1}). \tag{24}$$

3   Figure 8A indicates that the reaction of O with NO had the highest rate coefficient. Eq. 25

4   was utilized to compare the contribution of oxygen consumption for the above three reactions:

$$\alpha_3 = \frac{-r_{O_1}}{-r_{O_1} + -r_{O_2} + -r_{O_3}} = \frac{k_{O_1}[NO]}{k_{O_1}[NO] + k_{O_2}[O] + k_{O_3}[O_2]}. \tag{25}$$

5   where the ratio α_3 means the dominating reaction of oxygen consumption for Eqs. 19~21 at

6   different temperatures.

7   Figure 8B shows that the ratio α_3 was 99.1% at the calculated temperature of 2400 K, when

8   the input gases was 50%/50% O_2/N_2. The results indicated that O was mainly used for the

9   formation of NO_2 (Eq. 19), which led to an increase of NO_2 with energy density. Moreover, it

10   was noted that the produced NOx may be further reacted to subsequently reactions involving

11   NO_3 and N_2O_5. These reactions involving NO_3 and N_2O_5 somewhat increase the oxidation, but

12   this increase is within the uncertainty of measurements and reaction constants [32,33]. Thus,

13   the other possible reaction products were neglected in this study.

14

16
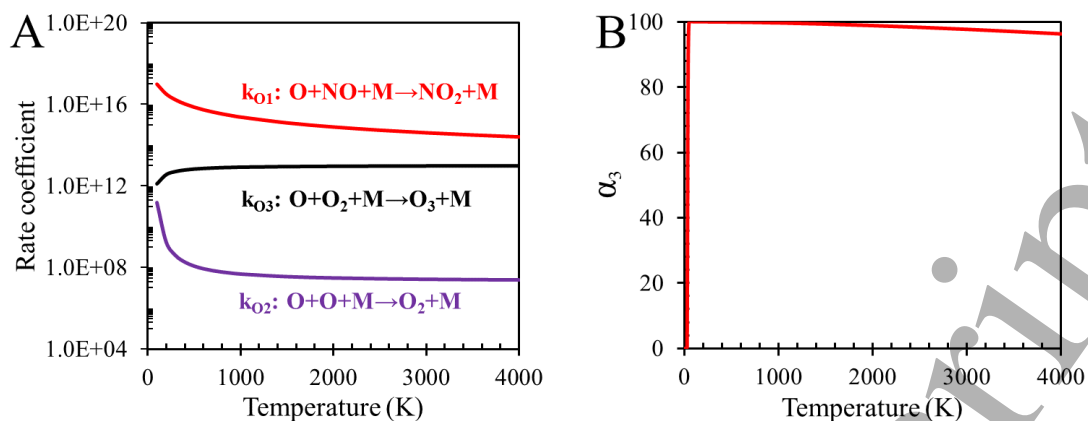
Figure 8. (A) Rate coefficients of Eqs. (19)~(21) plotted as functions of temperature and (B) corresponding reaction rate ratio at different temperatures.

4. Conclusion

The pulsed spark discharges for NOx production using the PTP and CTP plasma reactors at different energy densities were investigated. NOx can be produced with a high energy efficiency of 0.09 mol/kWh under the gases of 50%/50% N_2/O_2, while the NO_2 selectivity increased with increasing energy density. Moreover, the temperatures of the gases in the spark channels were estimated using the Gibbs free energy equation. The reactions of N with O_2 and O with NO were the major reactions for the NOx production.

17

1   **References**

2   [1] Bourke P, Ziuzina D, Boehm D, Cullen P J and Keener K 2018 The potential of cold plasma

3   for safe and sustainable food production *Trends Biotechnol.* **36** 615–26

4   [2] Patil B S, Cherkasov N, Lang J, Ibhadon A O, Hessel V and Wang Q 2016 Low temperature

5   plasma-catalytic NOx synthesis in a packed DBD reactor: Effect of support materials and

6   supported active metal oxides *Appl. Catal., B* **194** 123–33

7   [3] Maxwell G R 2012 Synthetic nitrogen products *Handbook of Industrial Chemistry and*

8   *Biotechnology* **22** 875–937

9   [4] Rouwenhorst K H R, Kim H H and Lefferts L 2019 Vibrationally excited activation of N_2 in

10   plasma-enhanced catalytic ammonia synthesis: A kinetic analysis *ACS Sustainable Chem.*

11   *Eng.* **7** 17515–22

12 [5] Barhoun P, Mehta P, Herrera F A, Go D B, Schneider W F and Hicks J C 2019

13   Distinguishing plasma contributions to catalyst performance in plasma-assisted ammonia

14   synthesis *ACS Sustainable Chem. Eng.* **7** 8621–30

15 [6] Pei X, Gidon D, Yang Y-J, Xiong Z and Graves D B 2019 Reducing energy cost of NOx

16   production in air plasmas *Chem. Eng. J.* **362** 217–28

17 [7] Cherkasov N, Ibhadon A O and Fitzpatrick P 2015 A review of the existing and alternative

18   methods for greener nitrogen fixation *Chem. Eng. Process.: Process Intensif.* **90** 24–33

19 [8] Du Z, Denkenberger D and Pearce J M 2015 Solar photovoltaic powered on-site ammonia

20   production for nitrogen fertilization. *Sol. Energy* **122** 562–8

[9] Rahman M, Cooray V, Montaño R, Liyanage P and Becerra M 2011 NOx production by impulse sparks in air *J. Electrost.* **69** 494–500

[10] Park S, Choe W and Jo C 2018 Interplay among ozone and nitrogen oxides in air plasmas: Rapid change in plasma chemistry *Chem. Eng. J.* **352** 1014–21

[11] Rehbein N and Cooray V 2001 NOx production in spark and corona discharges *J. Electrost.* **51-52** 333–9

[12] Sheng Z, Sakata K, Watanabe Y, Kameshima S, Kim H H, Yao S and Nozaki T 2019 Factors determining synergism in plasma catalysis of biogas at reduced pressure *J. Phys. D: Appl. Phys.* **52** 414002

[13] Sheng Z, Kameshima S, Yao S and Nozaki T 2018 Oxidation behavior of Ni/Al$_2$O$_3$ catalyst in nonthermal plasma-enabled catalysis *J. Phys. D: Appl. Phys.* **51** 445205

[14] Shao T, Wang R, Zhang C and Yan P 2018 Atmospheric-pressure pulsed discharges and plasmas: mechanism, characteristics and applications *High Volt* **3** 14–20

[15] Kim W, Do H, Mungal M G and Cappelli M A 2006 Flame stabilization enhancement and NOx production using ultra short repetitively pulsed plasma discharges *44th AIAA Aerospace Sciences Meeting and Exhibit*, AIAA 2006-560, Reno, NV

[16] Gao Y, Zhang S, Sun H, Wang R, Tu X and Shao T 2018 Highly efficient conversion of methane using microsecond and nanosecond pulsed spark discharges *Appl. Energy* **226** 534–45

[17] Yao S, Suzuki E, Meng N and Nakayama A 2002 A high-efficiency reactor for the pulsed plasma conversion of methane *Plasma Chem. Plasma Process.* **22** 225–37

[18] Yao S, Okumoto M, Madokoro K, Shimogami J, Suzuki E and Yashima T 2003 Plasma conversion of methane and CO_2 using a tubular circle-to-plate reactor *J. Chem. Eng. Jpn.* **36** 435–40

[19] Yao S, Nakayama A and Suzuki E 2001 Methane conversion using a high-frequency pulsed plasma: Important factors *AIChE J.* **47** 413–8

[20] Yao S, Nakayama A and Suzuki E 2001 Methane conversion using a high-frequency pulsed plasma: Discharge features *AIChE J.* **47** 419–26

[21] Yao S, Suzuki E and Nakayama A 2001 The pyrolysis property of a pulsed plasma of methane *Plasma Chem. Plasma Process.* **21** 651–63

[22] Janda M, Martisovits V, Hensel K and Machala Z 2016 Generation of antimicrobial NOx by atmospheric air transient spark discharge *Plasma Chem. Plasma Process.* **36** 767–81

[23] Fang P, Cen C, Tang Z, Zhong P, Chen D and Chen Z 2011 Simultaneous removal of SO_2 and NOx by wet scrubbing using urea solution *Chem. Eng. J.* **168** 52–9

[24] Saravanan S, Nagarajan G, Anand S and Sampath S 2012 Correlation for thermal NOx formation in compression ignition (CI) engine fuelled with diesel and biodiesel *Energy* **42** 401–10

1   [25] Yu L, Pierrot L, Laux C O and Kruger C H 1999 Effect of vibrational nonequilibrium on

2   the chemistry of two-temperature nitrogen plasma *14th International Symposium on*

3   *Plasma Chemistry*, Prague, Czech Republic

4   [26] Pierrot L, Yu L, Gessman R J, Laux C O and Kruger C H 1999 Collisional-radiative

5   modeling of nonequilibrium effects in nitrogen plasma *30th AIAA Plasmadynamics and*

6   *Lasers Conference*, *AIAA 1999-3478*, Norfolk, VA

7   [27] Hernandez J J, Lapuerta M and Perez-Collado J 2007 A combustion kinetic model for

8   estimating diesel engine NOx emissions *Combust. Theory Modell.* **10** 639–57

9   [28] Lu X P and Laroussi M 2008 Electron density and temperature measurement of an

10   atmospheric pressure plasma by millimeter wave interferometer *Appl. Phys. Lett.* **92**

11   051501

12   [29] Ono R and Oda T 2002 NO formation in a pulsed spark discharge in $N_2/O_2/Ar$ mixture at

13   atmospheric pressure *J. Phys. D: Appl. Phys.* **35** 543–8

14   [30] Bashtani J, Seddighi S and Bahrabadi-Jovein I 2018 Control of nitrogen oxide formation

15   in power generation using modified reaction kinetics and mixing *Energy* **145** 567–81

16   [31] Hori M 1980 Effects of probing conditions on NO_2/NOx ratios *Combust. Sci. Technol.* **23**

17   131–5

18   [32] Jõgi I, Levoll E and Raud J 2016 Plasma oxidation of NO in $O_2:N_2$ mixtures: The

19   importance of back-reaction *Chem. Eng. J.* **301** 149–57

1   [33] Chen J and Davidson J H 2002 Ozone production in the positive DC corona discharge:

2   Model and comparison to experiments *Plasma Chem. Plasma Process.* **22** 495–522

3